Thermochimica Acta, 27 (1978) 45–59

THERMAL DECOMPOSITION OF HYDROMAGNESITE $4MgCO_3 \cdot Mg(OH)_2 \cdot 4H_2O$ UNDER DIFFERENT PARTIAL PRESSURES OF CARBON DIOXIDE

YUTAKA SAWADA, KEIZO UEMATSU, NOBUYASU MIZUTANI AND MASANORI KATO*

Department of Inorganic Materials, Faculty of Engineering, Tokyo Institute of Technology, O-okayama, Meguro-ku, Tokyo 152, (Japan)

(Received 1st February 1978)

ABSTRACT

The thermal decomposition of hydromagnesite, $4MgCO_3 \cdot Mg(OH)_2 \cdot 4H_2O$, was studied under two typical experimental conditions; the condition in which an exothermic phenomenon at ~520 °C was absent (P_{CO_2} = 0.00 atm) and the one in which it was present (P_{CO_2} = 0.50 atm).

The specimen formed an amorphous phase including a lower carbonate intermediate after dehydration was completed at ~300 °C. At P_{CO_2} = 0.00 atm, decarbonation proceeded and MgO was formed at ~500 °C. At P_{CO_2} = 0.50 atm, crystallization of $MgCO_3$, the evolution of heat and a rapid evolution of carbon dioxide took place coincidentally at ~520 °C. The $MgCO_3$ was decomposed at higher temperatures.

A model was proposed to explain the exothermic phenomenon; the crystallization of $MgCO_3$ was assumed to cause the rapid evolution of heat which decomposed the specimen and generated the rapid gas evolution when the specimen powder was packed tightly.

INTRODUCTION

The thermal decomposition of hydromagnesite, $4MgCO_3 \cdot Mg(OH)_2 \cdot 4H_2O$, proceeds via dehydration and decarbonation to MgO. A curious exothermic phenomenon was found at ~500 °C in the decarbonation process. The decomposition process, especially the exothermic phenomenon, was strongly affected by the experimental conditions. In a previous paper[1], the necessary conditions for the occurrence of the exothermic phenomenon were established; a high partial pressure of carbon dioxide (P_{CO_2}) was required.

The exothermic phenomenon was explained by various mechanisms. Dell and Weller[2] and Morandi[3] proposed the crystallization of $MgCO_3$ since they detected the

* To whom correspondence should be addressed.

X-ray diffraction pattern of $MgCO_3$ in the specimen quenched immediately after the exothermic phenomenon took place. Tomizawa et al.[4] showed the correlation between the intensity of the exothermic peak and those of the $MgCO_3$ X-ray diffraction peaks. Beck[5] and Hashimoto et al.[6] proposed the crystallization of MgO from their results of X-ray diffraction on the quenched specimen. Hashimoto et al.[6] and Höland and Heide[7] reported the rapid evolution of carbon dioxide at ~500 °C. Recently, Suzuki et al.[8] detected the evolution of carbon monoxide from hydromagnesite, in amounts which were much greater than expected from the equilibrium between CO_2, CO and O_2. They explained that the crystallization of $MgCO_3$ triggered explosive combustion of carbon monoxide causing the exothermic phenomenon.

In the present paper, the thermal decomposition process was studied by comparing the structural changes under two typical experimental conditions; the condition in which the exothermic peak was absent (P_{CO_2} = 0.00 atm) and the one in which it was present (P_{CO_2} = 0.50 atm). The specimens were heated in the apparatus of differential thermal gas analysis (DTGA) in flowing helium–carbon dioxide mixed atmospheres and quenched from various temperatures for powder X-ray diffraction, infrared spectrum and compositional analyses. The carbon monoxide evolved from the specimen was measured quantatively.

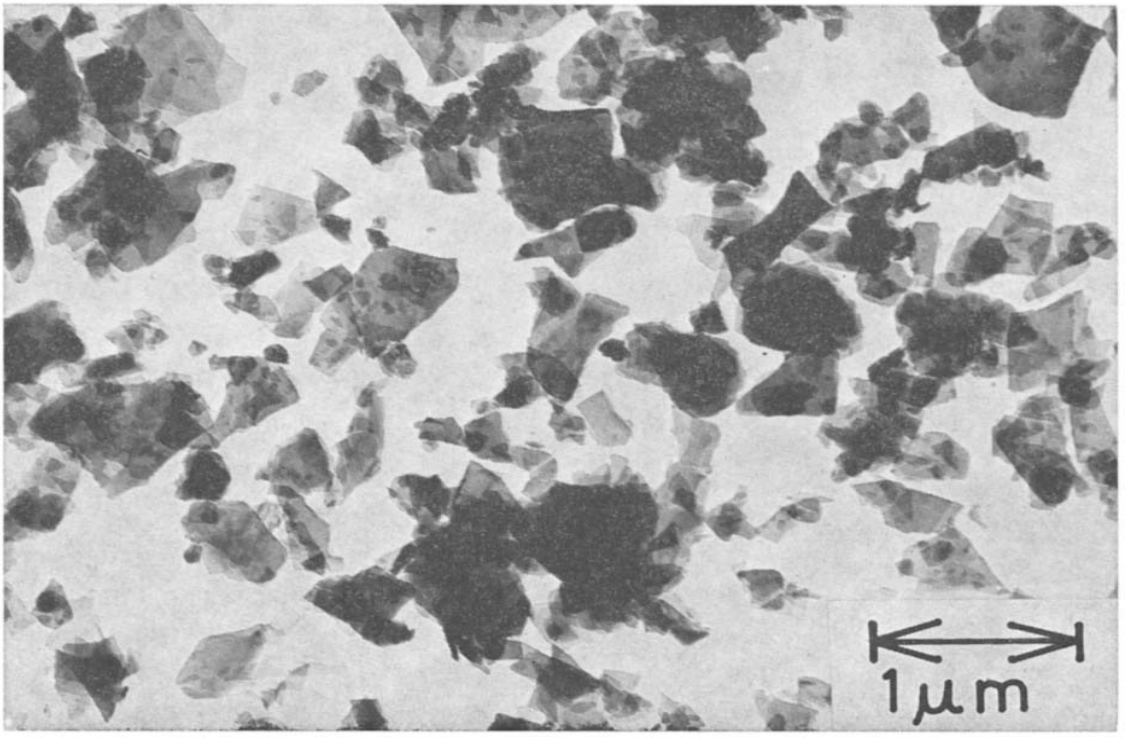

Fig. 1. Transmission electron micrograph of hydromagnesite.

EXPERIMENTAL

Specimen

Reagent grade basic magnesium carbonate (Wako Pure Chemical Industries, Ltd., Japan) was used. The $MgO:CO_2:H_2O$ ratio (1.00:0.75:0.96) from the compositional analysis was only slightly different from that of the pure hydromagnesite $4MgCO_3 \cdot Mg(OH)_2 \cdot 4H_2O$ (1.00:0.80:1.00). The X-ray diffraction pattern showed broad peaks from which the crystallite size, ~200–1000 Å, was estimated. The *d*-spacings agreed with the reported indices for hydromagnesite[9]. The specimen was a platelet of ~0.2–1.0 μm in length. Electron diffraction revealed that each particle was polycrystalline. The transmission electron micrograph of the specimen is presented in Fig. 1.

Differential thermal gas analysis

The DTGA was developed by Mizutani and Kato[10]. The reactor gas was prepared from helium and carbon dioxide in a gas mixing apparatus with partial pressure of carbon dioxide (P_{CO_2}) of 0.00–1.00 atm, a total pressure of 1.0 atm and a flow rate of 30 ml/min. The specimen was heated in the gas stream at a heating rate of 8.9 °C/min. Gas evolution from the specimen was determined in situ from the change of the thermal conductivity of the reactor gas. A trap (P_2O_5 or NaOH) could be inserted before the thermal conductivity detector in the gas flow system to determine the gas species in the evolved gas.

To study the effect of packing, the specimen was placed in two ways. In the first, which was the one used for the most part in this study, the specimen was placed in a platinum container. The reactor gas was passed over the specimen. In the second method, the specimen (~25 mg) was dispersed in silica wool and was placed in a platinum tubular container (5 mm diam. × 30 mm). The gas was passed through the container.

The specimen was quenched from the various temperatures during the heating process for powder X-ray diffraction, infrared spectrum and compositional analyses.

Differential thermal analysis and thermogravimetry

The decomposition process was studied with a DTA–TG apparatus (type M8076, Rigaku Denki Co., Japan) in a carbon dioxide atmosphere with specimen weight of 7.5 mg, a P_{CO_2} of 1.00 atm, a total pressure of 1.0 atm, a flow rate of ~30 ml/min and a heating rate of 10 °C/min.

Powder X-ray diffraction analysis

The structural changes of the quenched specimen were examined by a powder X-ray diffractometer (Philips Co.) with a Cu target, a Ni filter and a scanning speed 2θ = 2.0°/min. The crystallite sizes were estimated from the peak widths by Jones' method[11]. The lattice strain was neglected. MgO prepared by decomposing hydromagnesite at 1100 °C for 1 h was used as a standard.

Infrared spectrum analysis

The infrared spectrograph was recorded at room temperature on an IR-G type of Japan Spectroscopic Co., Japan. Approximately 0.1 mg specimen was mixed with ~200 mg KBr and pressed into a pellet. References were natural magnesite (Korea) and MgO prepared by calcining the hydromagnesite at 1100 °C.

Compositional analyses

The carbon contents of the decomposed specimens were measured with a C-elementary analysis apparatus. The specimen was heated at 850 °C for 5 min in a helium–oxygen mixture (mixing ratio 9:1) and the amount of carbon dioxide were quantitatively measured with a gas chromatograph.

Carbon monoxide analyses

The concentration of carbon monoxide in the reactor gas from the DTGA was determined after the water vapor was removed with a P_2O_5 trap, with a Kitagawa-type gas detective tube (No. 106FB, Komyo Rikagaku Industry Co., Japan) and a calcia-stabilized zirconia oxygen sensor (CSZ) operated at ~850 °C.

In the first method, the gas was introduced to a column filled with a carbon monoxide-sensitive reagent, $K_2Pd(SO_3)_2$. Carbon monoxide absorbed by the reagent changes its color from white to yellow forming a boundary or color change. After a specified period, the gas flow was switched to a new column; altogether 7 columns were used. The amount of carbon monoxide in each column was determined from the colored region of the reagent.

In the second method, the carbon monoxide concentration was measured indirectly; evolution of carbon monoxide from the specimen affects the equilibrium

$$CO_2 \rightleftarrows CO + \tfrac{1}{2} O^2$$

in the reactor gas (CO_2 + He), changing the EMF of the CSZ cell. The amount of carbon monoxide was estimated using a predetermined relation between the EMF and the concentration of carbon monoxide in the gas.

No carbon monoxide was detected in a blank test by either method. The detectors were calibrated with known amounts of carbon monoxide prepared by the decomposition of $CaC_2O_4 \cdot 3H_2O$ at ~400 °C.

To obtain a more generalized knowledge on the carbon monoxide evolved in the decarbonation process, a few types of carbonate compound (precipitated calcium carbonate, super reagent grade, Wako Pure Chemical Industries Ltd., Japan and natural magnesite from Korea) were decomposed under similar experimental conditions.

RESULTS

Thermal analyses

DTGA results for two typical decomposition processes are shown in Fig. 2A and B. A P_2O_5 trap absorbed the gas evolved from the specimen at ~100–300 °C.

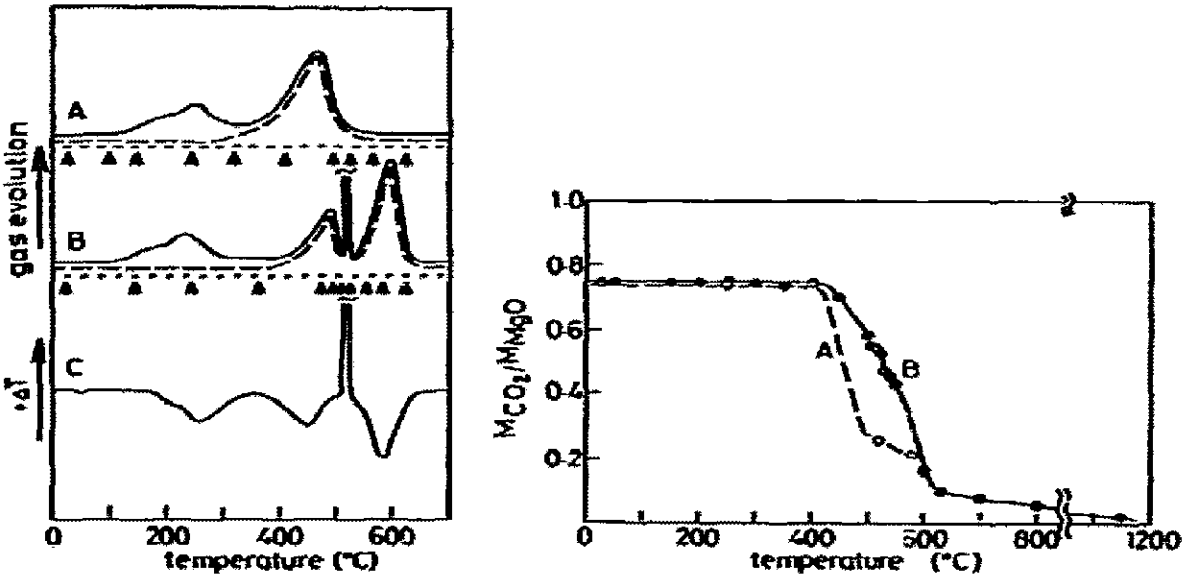

Fig. 2. Differential thermal gas analysis (DTGA) and differential thermal analysis (DTA) for hydromagnesite at various partial pressures (P_{co_2}) of carbon dioxide.
hydromagnesite at various partial pressures (P_{co_2}) of carbon dioxide. Atmosphere, mixture of helium and carbon dioxide; total pressure, 1.0 atm; gas flow rate, 30 ml/min.
A and B, DTGA (specimen weight, 25 mg; heating rate, 8.9 °C/min; A, P_{co_2} = 0.90 atm; B, P_{co_2} = 0.50 atm. ———, No trap inserted before the thermal conductivity detector; — —, P_2O_5 trap inserted; - - -, NaOH trap inserted; ▲, quenching temperature for powder X-ray diffraction analysis and infrared spectroscopy. The gas evolved at ~100–300 °C was water vapor and that at ~350–650 °C was carbon dioxide. C, DTA (specimen weight, 7.5 mg; heating rate, 10 °C/min; P_{co_2} = 1.00 atm).

Fig. 3. Analytical CO_2/MgO molar ratio for decomposed hydromagnesite. Specimen weight, 45 mg; heating rate, 8.9 °C/min; gas flow rate, 30 ml/min. M_{co_2} = molar amount of CO_2 in the specimen; M_{MgO} = molar amount of MgO in the specimen. A, helium atmosphere, P_{co_2} = 0.00 atm; B, helium–carbon dioxide mixed atmosphere, P_{co_2} = 0.50 atm.

A NaOH trap absorbed the gas evolved both at ~100–300 °C and ~300–650 °C. Dehydration took place at ~100–300 °C and decarbonation at ~300–650 °C. The amounts of carbon in the specimen quenched from various temperatures are shown in Fig. 3. Results of DTGA were in good agreement with those of the compositional changes, the weight loss of the quenched specimens and thermogravimetry.

The decarbonation was strongly affected by P_{co_2}. At low P_{co_2} (Fig. 2A), only one decarbonation peak appeared in DTGA. At high P_{co_2} (Fig. 2B), three decarbonation stages could be distinguished, ~350–510 °C, ~520 °C and ~530–650 °C. The relative amount of gas evolved in each stage was approximately 35:5:60.

Results of DTA under the same experimental conditions as those shown in Fig. 2B are presented in Fig. 2C. The evolutions of carbon dioxide at ~350–510 °C and ~530–650 °C were endothermic and the peak temperatures increased with increasing P_{co_2}. The rapid evolution of carbon dioxide was accompanied by a sharp exothermic peak in DTA. This peak temperature was approximately constant with P_{co_2}. The peak temperature vs. P_{co_2} is presented in Fig. 4. It should be noted that the

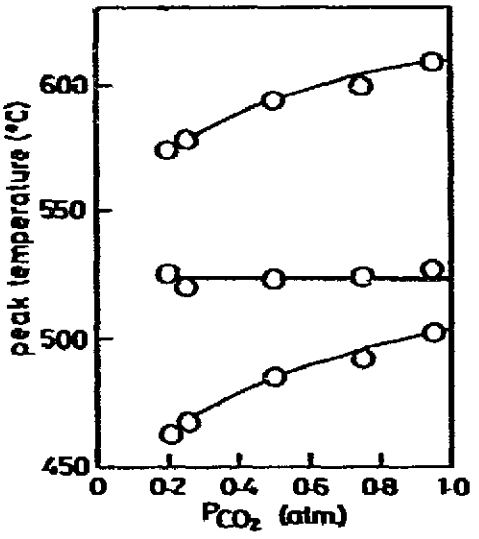

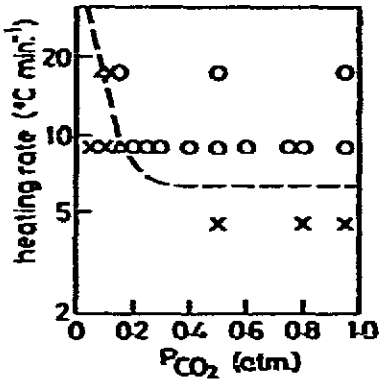

Fig. 4. Peak temperature of differential thermal gas analysis (DTGA) vs. partial pressure of carbon dioxide (P_{CO_2}) for hydromagnesite. Specimen weight, 25 mg; heating rate, 8.9 °C/min; atmosphere, mixture of helium and carbon dioxide; total pressure, 1.0 atm; gas flow rate, 30 ml/min. Only the peaks corresponding to evolution of carbon dioxide at $P_{CO_2} \geq 0.20$ atm are indicated.

Fig. 5. Heating rate vs. partial pressure of carbon dioxide (P_{CO_2}) and the occurrence of rapid gas evolution for hydromagnesite. ○, Rapid gas evolution occurred at 520 °C; △, only a trace appeared; X, no trace appeared.

temperature dependence of the peak at ~520 °C was different from those at ~350–510 °C and ~530–650 °C. The complication in the DTGA profile was observed at P_{CO_2} = ~0.05–0.15 atm.

The effects of P_{CO_2} and the heating rate on the occurrence of the rapid gas evolution is shown in Fig. 5. High P_{CO_2} and high heating rate was favorable for rapid gas evolution.

Rapid gas evolution did not take place in the specimen dispersed in silica wool. There was no other noticeable difference in the profile of the DTGA curve.

Decomposition at P_{CO_2} = 0.00 atm

X-Ray powder diffraction X-Ray powder diffraction patterns on the quenched specimens in a helium atmosphere (P_{CO_2} = 0.00 atm) are given in Fig. 6. No change was found under ~100 °C while no decomposition started. As dehydration proceeded at ~100–300 °C, the specimen retained hydromagnesite structures. However, peak broadening and decrease in the peak intensity were observed. When the dehydration was completed at ~300 °C, an amorphous diffraction pattern was observed. As decarbonation proceeded at ~300–450 °C, the specimen retained an amorphous pattern. A non-crystalline pattern was found by electron diffraction. Finally, faint MgO peaks appeared at ~500 °C when decarbonation was completed. The peaks became sharper and stronger as the temperature increased. The $MgCO_3$ pattern was never detected throughout the decomposition process in a helium atmosphere.

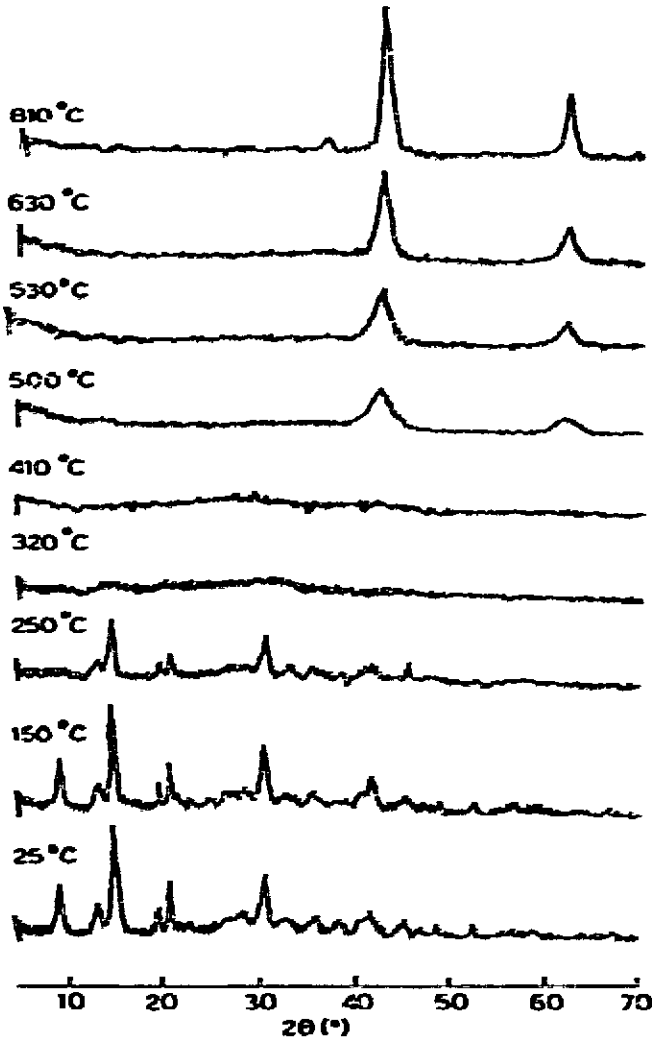

Fig. 6. X-Ray powder diffraction patterns for hydromagnesite decomposed in a helium atmosphere.

Infrared spectra Infrared spectra on the quenched specimens in a helium atmosphere (P_{CO_2} = 0.00 atm) are shown in Fig. 7. Hydromagnesite showed a pair of strong splits assigned to CO_3^{2-} ν_3 asymmetric stretching vibrations at ~1420–1480 cm^{-1} (12–15), three absorption bands assigned to CO_3^{2-} bending vibrations at ~800, ~850 and ~880 cm^{-1} (13–15), of which the one at ~800 cm^{-1} was the strongest (16), and an absorption band at ~1120 cm^{-1} assigned to CO_3^{2-} ν_1 symmetric stretching vibration (12). The absorption at ~2900–3700 cm^{-1} due to H_2O or OH vibrations (12) is not discussed in the present paper since no significant change was found. No change was found up to ~100 °C. As dehydration proceeded at ~100–300 °C, the hydromagnesite spectrum was retained, but the three absorption bands at ~800, ~850 and ~800 cm^{-1} and the pair of splits at ~1420–1480 cm^{-1} became gradually obscure. At 300 °C, where the dehydration was completed, the absorption band at ~580 cm^{-1} had disappeared and the pair of splits changed into one absorption band. As decar-

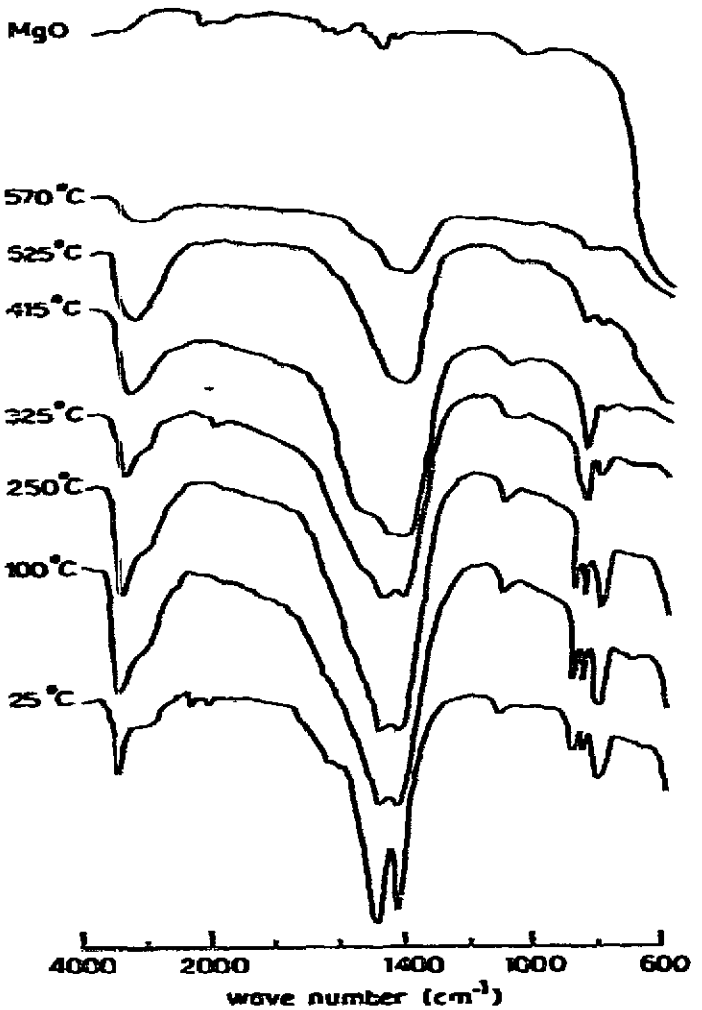

Fig. 7. Infrared spectra for hydromagnesite decomposed in a helium atmosphere. The spectrum of MgO, prepared by calcining the hydromagnesite at 1100 °C, is presented for reference.

bonation proceeded at ~300–500 °C, only one of the three absorption bands (~850 cm^{-1}) was retained at 415 °C, suggesting an increase of symmetry in the carbonate radical. A new absorption band appeared at ~1500 cm^{-1}, close to the position where the pair of splits at ~1420–1480 cm^{-1} had once existed. This spectrum was different from that of $MgCO_3$. In the following, this phase will be referred to as the "lower carbonate phase". The spectrum at 325 °C showed the intermediate of the hydromagnesite and the lower carbonate phase. The spectrum was similar to that of MgO after the decarbonation was completed at 500 °C. The $MgCO_3$ spectrum was never observed throughout the decomposition process in this atmosphere.

Decomposition at $P_{CO_2} = 0.50$ atm

X-Ray powder diffraction X-Ray powder diffraction patterns of the quenched specimens in a helium–carbon dioxide atmosphere ($P_{CO_2} = 0.50$ atm) are given in

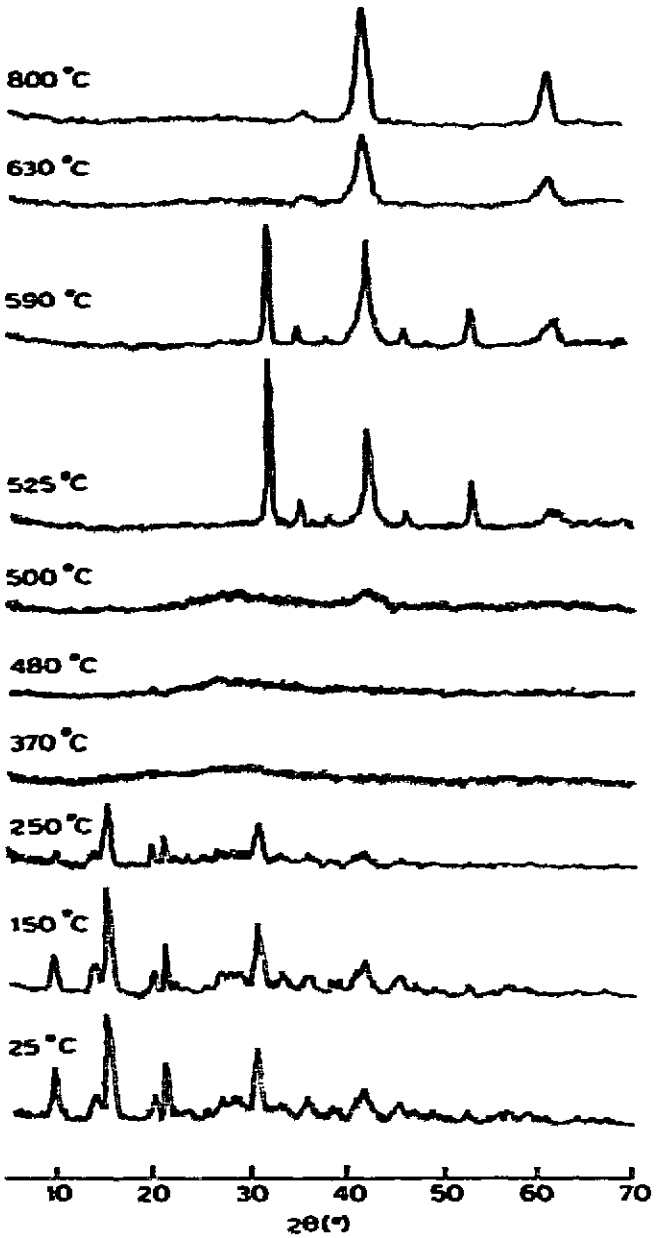

Fig. 8. X-Ray powder diffraction patterns for hydromagnesite decomposed in a helium–carbon dioxide mixed atmosphere (P_{CO_2} = 0.50 atm).

Fig. 8. The decomposition behavior was same as that in a helium atmosphere up to ~300 °C where dehydration was completed with an amorphous X-ray pattern. The amorphous pattern was preserved while decarbonation proceeded at ~400–500 °C. At the end of the decarbonation process (~500 °C), two faint broad peaks corresponding to the (200) and (220) diffraction of MgO (2θ = 42.94 and 62.68°) appeared. The specimen quenched immediately after the rapid evolution of carbon dioxide showed the $MgCO_3$ pattern (525 °C). As the decarbonation proceeded at higher temperature, the $MgCO_3$ diffraction peaks became weaker and broader. The skirt of

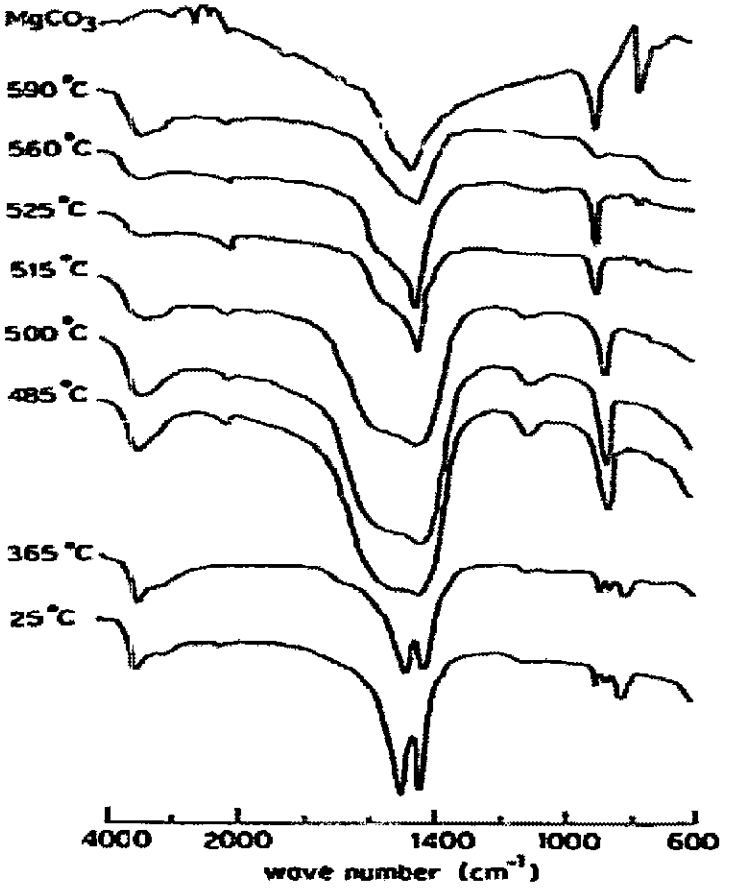

Fig. 9. Infrared spectra for hydromagnesite decomposed in a helium–carbon dioxide mixed atmosphere (P_{CO_2} = 0.50 atm). The spectrum of $MgCO_3$ is presented for reference.

$MgCO_3$ diffraction peak at 43.02° was broadened by virtue of the superimposed faint MgO diffraction peak at 42.94°. The $MgCO_3$ diffraction peaks at 61.39, 62.40 and 65.44° could not be separated from the background of the MgO diffraction peak at 62.68°. The MgO pattern was clearly observed after the decarbonation was completed above 630 °C; MgO diffraction peaks became sharper and stronger with increasing temperature.

The specimen dispersed in silica wool and quenched from 520 °C showed the $MgCO_3$ diffraction pattern.

Infrared spectra Infrared spectra on the quenched specimens in a helium–carbon dioxide atmosphere (P_{CO_2} = 0.50 atm) are shown in Fig. 9. The process was the same as that in a helium atmosphere up to ~300 °C where the dehydration was completed with the hydromagnesite spectrum with three absorption bands at ~800, ~850 and ~880 cm^{-1} and a slightly obscure pair of splits at ~1420 and ~1480 cm^{-1}. Dehydration did not affect the absorption of the carbonate radicals. As decarbonation proceeded at ~400–510 °C, the spectrum of the lower carbonate phase was observed

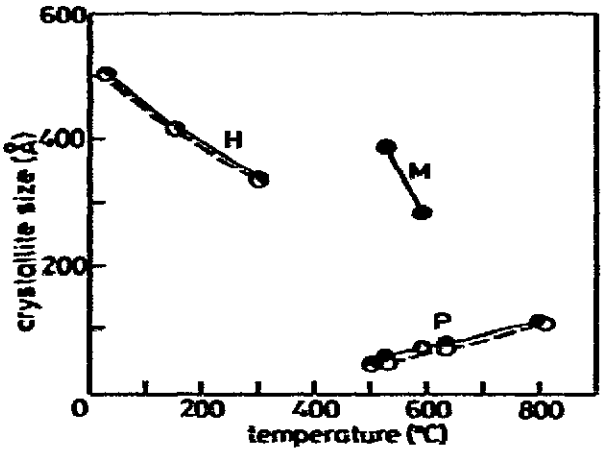

Fig. 10. The crystallite sizes for the decomposed hydromagnesite. ○, - - -. Helium atmosphere. P_{CO_2} = 0.00 atm; ●, ———. helium-carbon dioxide mixed atmosphere. P_{CO_2} = 0.50 atm. H. Hydromagnesite ($4MgCO_3 \cdot Mg(OH)_2 \cdot 4H_2O$); M. magnesite ($MgCO_3$); P. periclase (MgO). The crystallite sizes were determined from the peak widths of the X-ray diffraction peaks.

more clearly than in a helium atmosphere. A noticeable change in the intensity was found after this stage. The specimen quenched immediately after the rapid evolution of carbon dioxide (~525 °C) showed a new spectrum which was identified as $MgCO_3$. The absorption band at ~880 cm^{-1} was assigned to r_2 out-of-plane bending vibration of CO_3^{2-} in $MgCO_3$, the absorption band at ~1420 cm^{-1} to r_3 asymmetric vibration of CO_3^{2-} in $MgCO_3$ and that at ~740 cm^{-1} to r_4, planar bending vibration of CO_3^{2-} in $MgCO_3$ although the intensity was weak. The absorption band of the lower carbonate spectrum at ~1500 cm^{-1} disappeared but that at ~1420 cm^{-1} was preserved. The absorption band at ~850 cm^{-1} in the lower carbonate spectrum disappeared and instead the absorption band at ~880 cm^{-1} appeared, suggesting the increase of force constant for CO_3^{2-} r_2 out-of-plane bending vibration. The absorption band at ~1120 cm^{-1}, assigned to CO_3^{2-} r_1 symmetric stretching vibration (12) in hydromagnesite and the lower carbonate, was not found in $MgCO_3$. When the decarbonation was completed above ~600 °C, the $MgCO_3$ spectrum disappeared and the spectrum became similar to that of MgO.

The $MgCO_3$ spectrum was also observed in the specimen which was dispersed in silica wool and was quenched from ~520 °C.

The crystallite sizes for the decomposed specimens are given in Fig. 10. The crystallite sizes for hydromagnesite and $MgCO_3$ decreased during the decomposition process although the deviations were large. The crystallite size of $MgCO_3$ (~400 Å), which appeared suddenly at ~520 °C, was approximately equal to those of hydromagnesite (~300–550 Å) but much greater than those of MgO (~50–110 Å). Grain growth of MgO was clearly observed above 500 °C. The grain growth behavior was independent of the partial pressure of carbon dioxide.

Results of the thermal decomposition processes are summarized in Fig. 11 for different partial pressures (P_{CO_2} = 0.00 and 0.50 atm) of carbon dioxide.

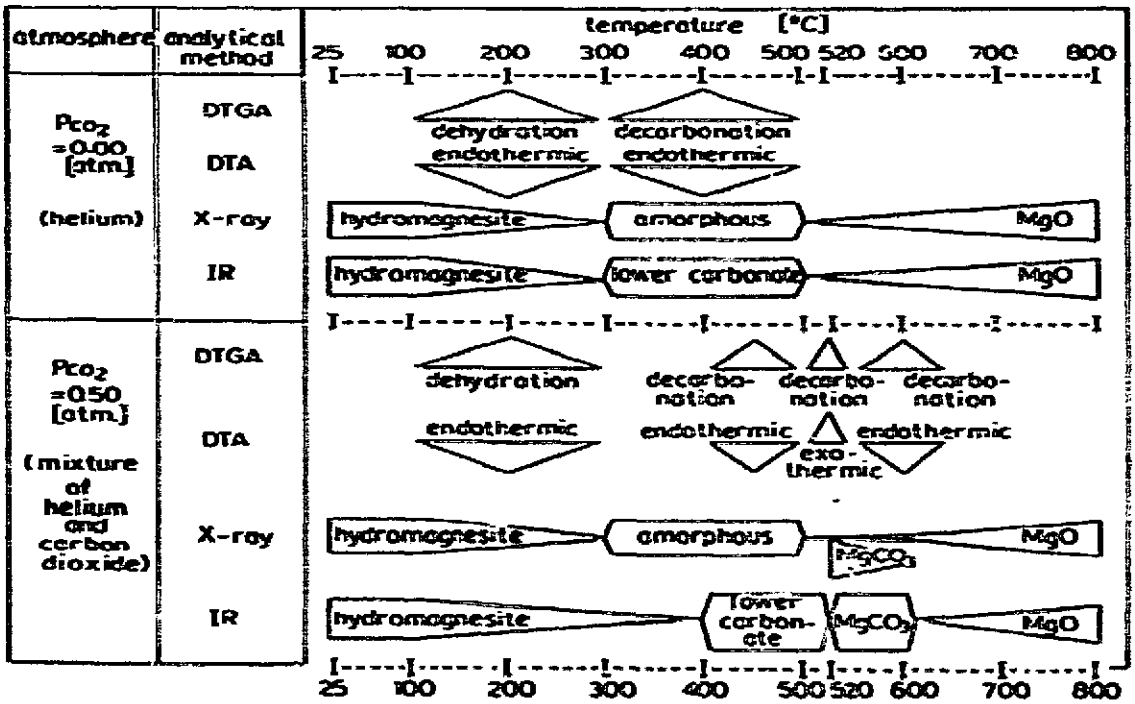

Fig. 11. Diagram for two typical thermal decomposition processes of hydromagnesite under different partial pressure of carbon dioxide.

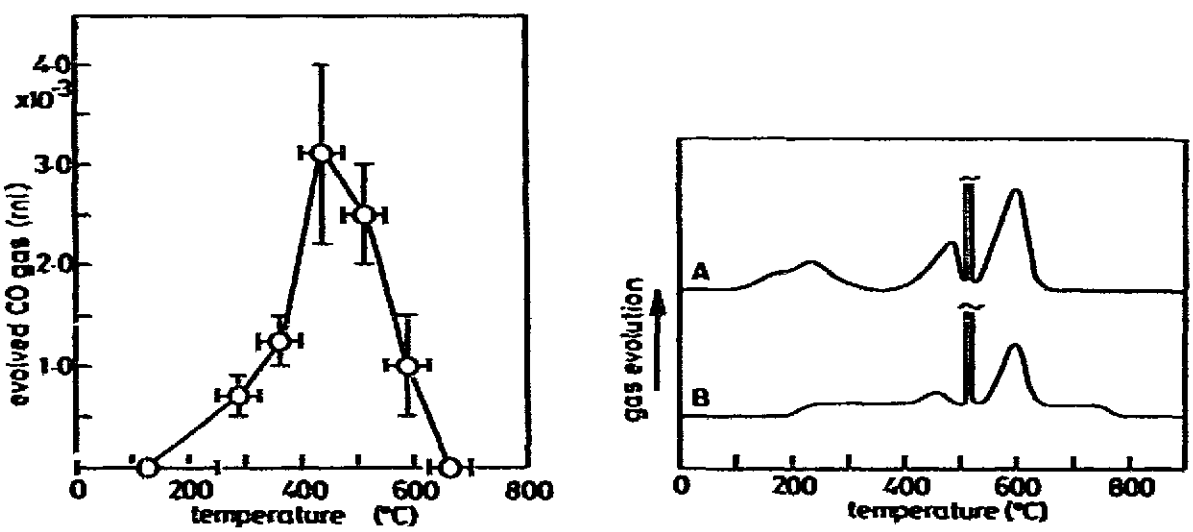

Fig. 12. Amount of carbon monoxide evolved from hydromagnesite determined with Kitagawa-type gas detection tube. Specimen weight, 150 mg; heating rate, 8.9 °C/min; atmosphere, mixture of helium and carbon dioxide; gas flow rate, 50 ml/min; P_{CO_2}, 0.50 atm. Each detector except the first was used for 7.5 min; only the integral amount during this period was determined. The horizontal line shows the temperature of the specimen in this period. The vertical line shows the inaccuracy in determining the amount of carbon monoxide from the color change. The first detector was used until the color change was formed in the column at 250 °C.

Fig. 13. Differential thermal gas analysis (DTGA) for hydromagnesite detected with thermal conductivity detector and calcia-stabilized zirconia cell oxygen sensor. A, Detected with thermal conductivity detector (TCD); B, detected with calcia-stabilized zirconia cell oxygen sensor. Specimen weight, 190 mg; heating rate, 8.9 °C/min; atmosphere, mixture of helium and carbon dioxide; P_{CO_2} = 0.50 atm.

Analysis on evolved carbon monoxide

The amount of carbon monoxide, measured with a Kitagawa type gas detection tube, is shown in Fig. 12 and that measured with a CSZ cell is shown in Fig. 13. In Fig. 13, the amount of carbon dioxide measured with a thermal conductivity detector is also presented. Carbon monoxide was evolved at ~200–750 °C. The decomposition process followed by both methods were essentially same. However, much more detailed information on the process was obtained by the method using a CSZ cell (Fig. 13). This method also enabled us to monitor the decomposition process continuously. Figure 13 shows that the carbon monoxide and carbon dioxide were evolved simultaneously and ratio of CO/CO_2 was approximately constant at ~400–650 °C. The apparent evolution of carbon monoxide at the high temperature (≥ 650 °C in Fig. 13) was due to fluctuation of the instrument. The evolution of carbon monoxide at low temperature (≤ 400 °C) was not accompanied by the evolution of carbon dioxide. The actual value of the ratio was estimated from the result shown in Fig. 12 and the peak area in Fig. 13. Both methods gave essentially the same results (~1/1000). The ratios in other carbonate compounds ($CaCO_3$ and $MgCO_3$) were found to be approximately constant (~1/1000).

DISCUSSION

The rate of decarbonation was reduced by a high P_{CO_2}. High P_{CO_2} applied externally was the simplest case. In addition to this, high P_{CO_2} was also created around the specimen (so-called self-generated atmosphere) when the specimen powder was densely packed or the heating rate exceeded the rate of ventilation. High heating rate also shortened the effective period for time-dependent decomposition processes, such as diffusion, to occur, and a large part of the specimen was preserved without decomposition up to higher temperature.

The composition of the specimen at ~500 °C at P_{CO_2} = 0.50 atm was approximately 2.6 ($MgCO_3$) · 3.2 (MgO). Faint X-ray diffraction peaks of MgO at ~500 °C indicates that the specimen at this temperature was heterogeneous, consisting of crystalline MgO (crystallite size ~50 Å) and an amorphous phase including magnesium carbonate. The structure of the amorphous carbonate is only partially understood. High symmetry of CO_3^{2-} ion similar to that of $MgCO_3$ was expected since only one CO_3^{2-} ν_2 out-of plane bending vibration was observed in the infrared spectrum, while hydromagnesite showed three ν_2 vibration modes. However, the force constant of CO_3^{2-} in the amorphous carbonate was lower than that in $MgCO_3$. The high crystallization rate of $MgCO_3$ indicates that only short-range transport of ions was involved in the process. This is consistent with the results that $MgCO_3$ (crystallite size ~400 Å) was crystallized only from the amorphous phase of high CO_3^{2-} concentration.

It was concluded in our previous paper[1] that the process which leads to the exothermic phenomenon was initiated in a compressed specimen and was spread rapidly to the other parts of the specimen. When the specimen was placed under a

temperature gradient, the crystallization was initiated at a microregion where the temperature was maximum and the heat of crystallization was transferred to the other parts of the specimen to trigger the further crystallization in a very short period of time. When the specimen was dispersed in silica wool, the rapid evolution of carbon dioxide was not generated even though crystallization took place. It was explained in this case that the heat was transferred to the surroundings.

The rapid evolution of carbon dioxide is consistent with those reported by Hashimoto et al.[6] and Höland and Heide[7].

A set of phenomena, the evolution of heat and carbon dioxide and crystallization of $MgCO_3$, can be understood when the following steps are assumed.

(1) The transformation of $MgCO_3$ from the amorphous phase to the crystalline phase takes place with a substantial heat of crystallization.

(2) The temperature of the specimen increases sharply when the specimen is packed tightly. The temperature rise in the specimen dispersed in silica wool is much smaller since the heat of crystallization will diffuse away into the surrounding medium.

(3) The decomposition of fresh $MgCO_3$ is highly temperature dependent: a drastic increase in the decomposition rate resulted from a slight temperature rise in the specimen.

Occurrence of the crystallization of $MgCO_3$ was supported by the result of X-ray diffraction analysis on the specimens which were quenched before and after the evolution of heat and carbon dioxide. This result is also consistent with those of Dell and Weller[2], Morandi[3] and Tomisawa et al.[4]. The temperature at which the phenomenon took place was not affected by the partial pressure of carbon dioxide (Fig. 4). This result strongly suggests that the phenomenon is triggered not by a chemical reaction governed by the mass action law, but by a structural change. When the specimen was dispersed in silica wool, the crystallization of $MgCO_3$ took place without involving the set of phenomena.

The newly formed $MgCO_3$ did not decompose at ~520 °C. It decomposed rapidly at higher temperatures (~530-650 °C at P_{CO_2} = 0.50 atm) (Fig. 2B). It is therefore expected that the rapid evolution of carbon dioxide only takes place when the actual specimen temperature is in the temperature range for decarbonation mentioned above. The decarbonation process during the rapid gas evolution is probably same as that of the normal decarbonation reaction. The decomposition of carbonates is an endothermic reaction so that the heat of crystallization will also be offset by the rapid decarbonation.

Faint MgO peaks were observed at ~500 °C (Fig. 8) before the exothermic phenomenon. No significant increase of MgO peak intensity was found during the exothermic phenomenon. These results show that the crystallization of MgO is not responsible for the exothermic phenomenon. The results of Beck[5] and Hashimoto et al.[6] were questionable. They probably failed to quench the specimen at the right time.

Evolution of carbon monoxide was found, however, and the concentration was smaller than that reported by Suzuki et al.[8]. Approximately the same amount of car-

bon monoxide was found in the decomposition of $CaCO_3$ and $MgCO_3$ in our experiments. This suggests that the evolution of a minute amount of carbon monoxide is common in the thermal decomposition of carbonate compounds.

An analogous exothermic phenomenon was reported for nesquehonite $MgCO_3 \cdot 3H_2O$ (2, 3, 5 and 17–19) on which we will report in the near future.

ACKNOWLEDGEMENT

The authors thank Mr. T. Saito of the Laboratory of Resources Utilization, Tokyo Institute Technology for the compositional analyses.

REFERENCES

1 Y. Sawada, K. Yematsu, N. Mizutani and M. Kato, *J. Inorg. Nucl. Chem.*, 40 (1978) 979.
2 R. M. Dell and S. W. Weller, *Trans. Faraday Soc.*, 55 (1959) 2203.
3 N. Morandi, *Miner. Petrogr. Acta*, 15 (1969) 93.
4 T. Tomizawa, S. Hara and H. Hashimoto, *Yogyo Kyokai Shi*, 84 (1976) 259.
5 C. W. Beck, *Am. Mineral.*, 35 (1950) 985.
6 H. Hashimoto, T. Tomizawa and M. Mitomo, *Kogyo Kagaku Zasshi*, 71 (1968) 450.
7 W. Höland and K. Ueide, *Thermochim. Acta*, 15 (1976) 287.
8 J. Suzuki, M. Ito and T. Sugiyama, *J. Jpn. Assoc. Min. Petr. Econ. Geol.*, 70 (1975) 79.
9 Powder Diffraction File, Joint Committee on Powder Diffraction Standards, Swarthmore, U.S.A., 1977, Inorganic 8-179.
10 N. Mizutani and M. Kato, *Anal. Chem.*, 47 (1975) 1389.
11 F. W. Jones, *Proc. R. Soc. London, Ser. A*, 166 (1938) 376.
12 W. B. White, *Am. Mineral.*, 56 (1971) 46.
13 F. A. Miller and C. H. Wilkins, *Anal. Chem.*, 24 (1952) 1253.
14 G. Raade, *Am. Mineral.*, 55 (1970) 1457.
15 K. Nakamoto, *Kagaku No Ryoiki*, 14 (54) (1963) 67.
16 F. A. Mupton, H. W. Jaffe and C. S. Thomson, *Am. Mineral.*, 50 (1965) 1893.
17 S. Iwai, H. Murotani, H. Morikawa and H. Aoki, *Yogyo Kyokai Shi*, 77 (1969) 411.
18 A. Doi and C. Kato, *Kogyo Kagaku Zasshi*, 74 (1971) 1597.
19 J. Suzuki and M. Ito, *J. Jpn. Assoc. Min. Petr. Econ. Geol.*, 69 (1974) 275.